Review of New particle formation induced by anthropogenic-biogenic interactions in the southeastern Tibetan Plateau, Lai et al.

This manuscript contains a suite of high-quality measurement data showing H2SO4, HOMs, and a PNSD from the Tibetan plateau. Frequent NPF was observed and an analysis of both the measurement data and some very impressive WRF-Chem simulations are presented giving some fascinating insights into the chemistry on a larger scale than measurements allow. The WRF-Chem simulations are possible due to some improvements to the VBS. The methodology for both the measurements and model are, however, extremely sparse. The developments to VBS are not discussed at all, neither are the processing of the measurement data. Similarly, the analysis of the mass spectral data is not given enough time. Many of the key arguments depend on the HOMs being monoterpene oxidation products, but the mass spectra are not discussed in detail. I understand that this would result in a very large paper so I think these things belong in the supplement. Once these are addressed, I very highly recommend this for publication as it is an extremely impressive paper.

Response: We would like to thank the referee for providing the insightful suggestions, which indeed help us further improve the manuscript.

General comments

1) *The methodology regarding instrumentation is a little bit thin-on-the-ground. It would be nice to have more information about the equipment. What flow rates were the instruments run at? Did they share an inlet? Did the PSM run in scanning mode? What were the time resolution? How were the PTR and CIMS instruments calibrated? What about mass-dependent transmission corrections? This information can go in the supplement, but it is important.*

Response: Thanks for your comment. The particle number size distributions (PNSDs) in the size range from 1 nm to 20 μm were collectively measured using five instruments, including a Particle Size Magnifier (PSM, Airmodus Inc.), a Neutral cluster and Air Ion Spectrometer (NAIS, Ariel Inc.), two Scanning Mobility Particle Sizers (nano-SMPS and long-SMPS, TSI Inc.) and an Aerodynamic Particle Sizer (APS, TSI Inc.). The PSM was operated in the scanning mode, with the saturator flow rate continuously changing from 0.1 L/min to 1.3 L/min. The NAIS observed air ion number size distributions from 0.8 nm to 40 nm and particle number size distributions from 2 nm to 40 nm. The nano-SMPS and long-SMPS share similar configurations but differ by a differential mobility analyzer (DMA) and a condensation particle counter (CPC) for measuring PNSDs in the size range of 4–70 nm and 12–540 nm, respectively. The APS measures the PNSD from 500 nm to 20 μm in the aerodynamic diameter. The sample air of nano-SMPS, long-SMPS and APS were dried using the silica gel dryer. The inlet flow rate of PSM, NAIS, nano-SMPS, long-SMPS and APS were 2.5 L/min, 54 L/min, 1.5 L/min, 1 L/min and 5 L/min, respectively. Throughout the intensive campaign, nano-SMPS and long-SMPS shared one inlet tube while the other instruments used separated inlet tubes. The PNSD in the overlapping size ranges detected by different particle sizers demonstrated good agreement. To obtain the PNSD from 4 nm to 1000 nm, the SMPS data and APS data were merged by following the method described by Beddows et al. (2010). The time resolution of PSM, NAIS, nano-SMPS, long-SMPS and APS data were 4 min, 3.5 min, 5.5 min, 5.5 min and 5.5 min, respectively.

The monoterpene concentration was measured by a Proton Transfer Reaction Time-

Of-Flight Mass Spectrometer (PTR-TOF-MS, Ionicon Analytik Inc.). During the campaign, the transmission function of the PTR-TOF-MS was calibrated with a 15-component gas mixture standard that included isoprene, α-pinene, benzene, and toluene. A nitrate Chemical Ionization with the Atmospheric Pressure interface Time-Of-Flight mass spectrometer (CI-APi-TOF, Aerodyne Research Inc.) was used to detect the H_2SO_4 and HOMs (Jokinen et al., 2012). H_2SO_4 was calibrated during the campaign by utilizing a stable and adjustable concentration H_2SO_4 source (Kürten et al., 2012). The mass-dependent transmission correction of the CI-APi-TOF was determined by following the method described by Heinritzi et al. (2016), by depleting the reagent ions with several perfluorinated acids before the campaign.

To address your concern, we have included additional information regarding instrumentation (section S1) in the supplementary information section for further clarity.

2) *Comment: The improvements to WRF-Chem are very valuable! But barely discussed. You say you updated VBS to incorporate RO2 chemistry, including autoxidation and dimerization! Is this similar to existing work such as PRAM/autoPRAM? (1). This should definitely be discussed in detail (again, even if only in the supplement) as the outcomes of the paper hinge on these results. Also, are there plans to make these improvements available widely?*

Response: Thanks for your comment.

Previous studies have demonstrated that oxidation of monoterpene could generate large amounts of ultra- and extremely low-volatility organic compounds, which are important precursors for NPF (Ehn et al., 2014). Thus, in our study, the peroxy radicals (RO_2) chemistry we accounted for is specific to monoterpenes. The modified volatility basis set (VBS) framework we used in WRF-Chem explicitly represents peroxy radicals (RO_2) chemistry and distributes products into the appropriate volatility bins after RO_2 termination into stable molecules. In the modified VBS framework, organic species are lumped into the C* bins, with C* ranging from 10^{-9} to 10^5 μg m^{-3}, separated by powers of 10^2 (i.e., 8 bins in total).

The reactions begin with oxidation of monoterpene with O_3, OH, and NO_3, producing peroxy radicals (RO_2). The model distinguishes two types of peroxy radicals: one with the potential for autoxidation and the other without. The radical termination proceeds via unimolecular termination or reactions with HO_2, NO, or another peroxy radical. Peroxy radical cross-reactions can produce dimers (ROOR), and the fraction of dimers in all cross-reaction products is assumed to depend on the volatility of the reacting peroxy radicals. The non-dimer cross-reaction products, as well as the termination products via unimolecular termination or reaction with NO, undergo either functionalization or fragmentation. The reactions and rate coefficients in our work are summarized in Table S1 of Schervish and Donahue (2020). It is noteworthy that the mechanism of peroxy radical autoxidation used in this study was similar with that in PRAM/autoPRAM (Roldin et al., 2019), but it is a simplified version due to the computational efficiency of the regional transport model. We map the stable molecules generated from each peroxy radical termination pathway to a distribution of species in the VBS space through kernels, allowing us to represent the wide variety of both peroxy radicals and stabilization reactions (Schervish and Donahue, 2020). The kernels used in this work are summarized in Tables S3–S6 of Schervish and Donahue (2020).

To address your comment, we have added discussions in the supplementary information (section S2) to provide more details about the improvements made to the WRF-Chem model, especially regarding the updates to the VBS. Additionally, we want to clarify that the modified codes of WRF-Chem in this study are available

upon request to the corresponding authors.

3) *Similar to the previous comments, as your arguments hinge on the HOMs being monoterpene oxidation products, it would be nice if you showed them in more detail. The mass defect shows them, but you've lumped C6-10 together. Why not colour it by carbon number? I'd also like to see DBE per carbon, and average oxidation state. Otherwise I have no idea what the HOMs actually are. I'd need to be satisfied that the HOMs are similar to alpha-pinene oxidation products, as many of the later arguments depend on alpha pinene lab studies.*

Response: Thanks for your comment. We have modified the mass defect plot (Fig. 3c or Fig. R1c) in the revised manuscript, by colouring the values by carbon number. Fig. R1c shows the mass defect plots of negative ion cluster during the NPF period on 29 April. Many ions with m/z values higher than 300 Th and carbon number higher than 10 were observed during the NPF, suggesting the contribution of HOMs to the nucleation.

During 28-30 April, 2021, the median double bond equivalent (DBE) and DBE per carbon of neutral HOMs observed by CI-APi-TOF were 2.97 and 0.34, respectively. Moreover, the C10 HOMs dominated the carbon distribution of HOMs, with the fraction of 32%. All those evidences suggest that the HOMs are mainly formed by the oxidation of monoterpene oxidation. The detailed data analysis of CI-APi-TOF data (e.g. bin-PMF etc) is beyond the scope of this study. Our another work will focus on the pathway of HOMs formation from monoterpene oxidation in the southeastern part of Tibetan Plateau. Nevertheless, we have presented required results from CI-APi-TOF measurements to support that HOMs in the southeastern part of Tibetan Plateau are mainly from monoterpene oxidation in the revised manuscript (Lines 327-332).

We indeed improved the WRF-Chem model based on the mechanism of alpha-pinene oxidation, as a large number of lab experiments have thoroughly investigated this mechanism. Various monoterpenes including alpha-pinene, beta-pinene and limonene are grouped together in the WRF-Chem, which leads to the uncertainties in the modelling of HOMs. The yield of HOMs is higher for alpha-pinene than for beta-pinene, while lower than for limonene. In the revised manuscript, we have added the discussions on the model uncertainties in the supplementary information (section S2).

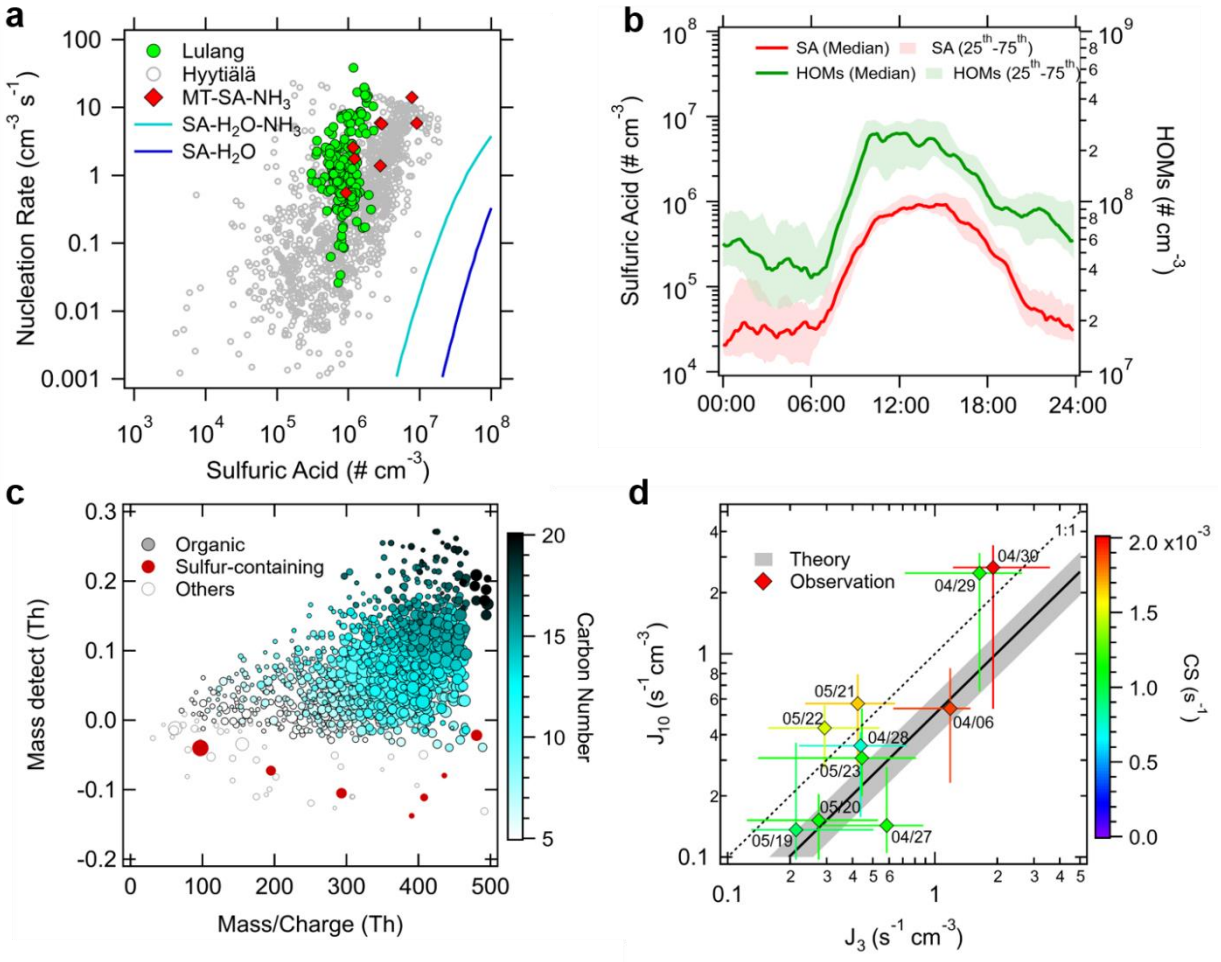

Fig. R1. (a) Nucleation rates ($J_{1.7}$) as a function of H_2SO_4 concentration at ambient observations in Lulang (green circles), Hyytiälä (gray circles) (Sihto et al., 2006; Kulmala et al., 2013) and CLOUD experiments (red diamonds) (Lehtipalo et al., 2018). The cyan and blue lines denote ternary (H_2SO_4-NH_3-H_2O) nucleation and binary nucleation (H_2SO_4- H_2O), respectively, based on CLOUD data in Kürten et al. (2016). (b) Averaged diurnal variations of H_2SO_4 concentrations and HOMs concentration on NPF days in Lulang. The solid lines are the median values and shaded areas denote the 25th or 75th percentiles. (c) A mass defect plot illustrating the chemical composition of negative ion clusters at 12:00 on 29 April. The size and color of symbol size correspond to the relative signal intensity on a logarithmic scale and carbon number, respectively. (d) Formation rate at 10 nm (J_{10}) versus formation rate at 3 nm (J_3) at ambient observations in Lulang (diamonds). Diamonds are color-coded by condensation sink. Error bars present the 25th - 75th percentiles. The solid grey line shows the relationship between J_{10} and J_3 based on theory (Kulmala et al., 2012) and the uncertainties are shown by the shaded bands. Dash 1:1 line is shown for reference.

Specific comments

1. Line 223: I'm not sure I understand the logic here, why only those species with C^* of 10^{-9} and 10^{-7}? Why not 10^{-8}? Surely this would avoid you having to input the factor-of-six adjustment?

Response: Thanks for your comment.

In this study, we aimed to encompass the broad volatility spectrum of organic vapors while balancing computational efficiency. To achieve this, biogenic organic species are lumped into eight volatility bins having saturation vapor concentrations

(C*) of 10^{-10}–10^{-9},10^{-8}–10^{-7},10^{-6}–10^{-5},10^{-4}–10^{-3},10^{-2}–10^{-1},10^{0}–10^{1},10^{2}–10^{3},10^{4}–10^{5} μgm^{-3}.

Lehtipalo et al. (2018) demonstrated that, among Highly Oxygenated Molecules (HOMs), only organic vapors with ultra-low or extremely low volatility are significant contributors to nucleation. Hence, in our model, surrogate species with C* values lower than 10^{-7} μgm^{-3} formed from monoterpene oxidation are considered as the nucleating vapors. Considering the referee's points, we clarified in the revised manuscript (Lines 249, 252).

2. Line 229: Can you explain the temperature dependence function?

Response: Thanks for your comment.

The temperature dependence function for organic nucleation in our study is derived from the work of Dunne et al. (2016).

Dunne et al. (2016) determined the temperature dependence through the Atmospheric Cluster Dynamics Code model (ACDC) studies based on quantum chemical calculations of cluster binding energies. They used the organic proxy compound 3-methyl-1,2,3-butane-tricarboxylic acid (MBTCA) for their calculations. MBTCA was chosen because it is a well-known compound formed in the oxidation of volatile organic compounds and has a high O:C ratio. The formation free energies for MBTCA-sulfuric acid clusters were already available from previous works (Riccobono et al., 2014).

However, it's important to note that this estimation could potentially lead to a stronger temperature dependence than reality. This is because the isomerization reactions that create organic molecules with sufficiently low volatility to participate in nucleation are slower at low temperatures. In these cases, instead of isomerization, organic peroxy radicals react with other peroxy radicals to create stable, less oxidized species, leading to a decrease in oxidation levels.

To address this, Dunne proposed a plausible weaker temperature dependence, which lies between the extremes of zero temperature dependence and the MBTCA case. The expression used for the temperature dependence is as follows:

$$Jorg' = Jorg \exp(-(T - 278)/10)$$

This formula represents the temperature dependence we apply in our model.

To address your concern, we have included additional information regarding the temperature dependence in the supplementary information (section S3) for further clarity.

3. Line 279: Not sure Qi and Riccobono are the right references here. Maybe these two: (2, 3) as the former shows the formation of particles primarily through HOMs, while the latter shows the importance of HOMs as well as H_2SO_4 + NH_3 in the boreal environment a little more accurately than Riccobono. Maybe also (4) to show their role in growth.

Response: Thanks for your comment. We have modified the references in the revised manuscript (Lines 313–314).

4. Figure 3: This figure is great. Is it possible to include one for the whole campaign including H2SO4 and HOM? Also maybe use a different colour palette other than Jet (maybe Turbo or Viridis). Same for the other figures.

Response: Thanks for your comment. We modified the Fig. 3a, by using Turbo colormap in the revised manuscript (Fig. R2). The time series of particle number size distribution from 1 nm to 1000 nm, ion number size distribution, SO_2, monoterpene, O_3, H_2SO_4 and HOMs during the whole campaign were presented in Supplemental Information (Fig. R3) and we added descriptions in the revised manuscript (Lines 291–292).

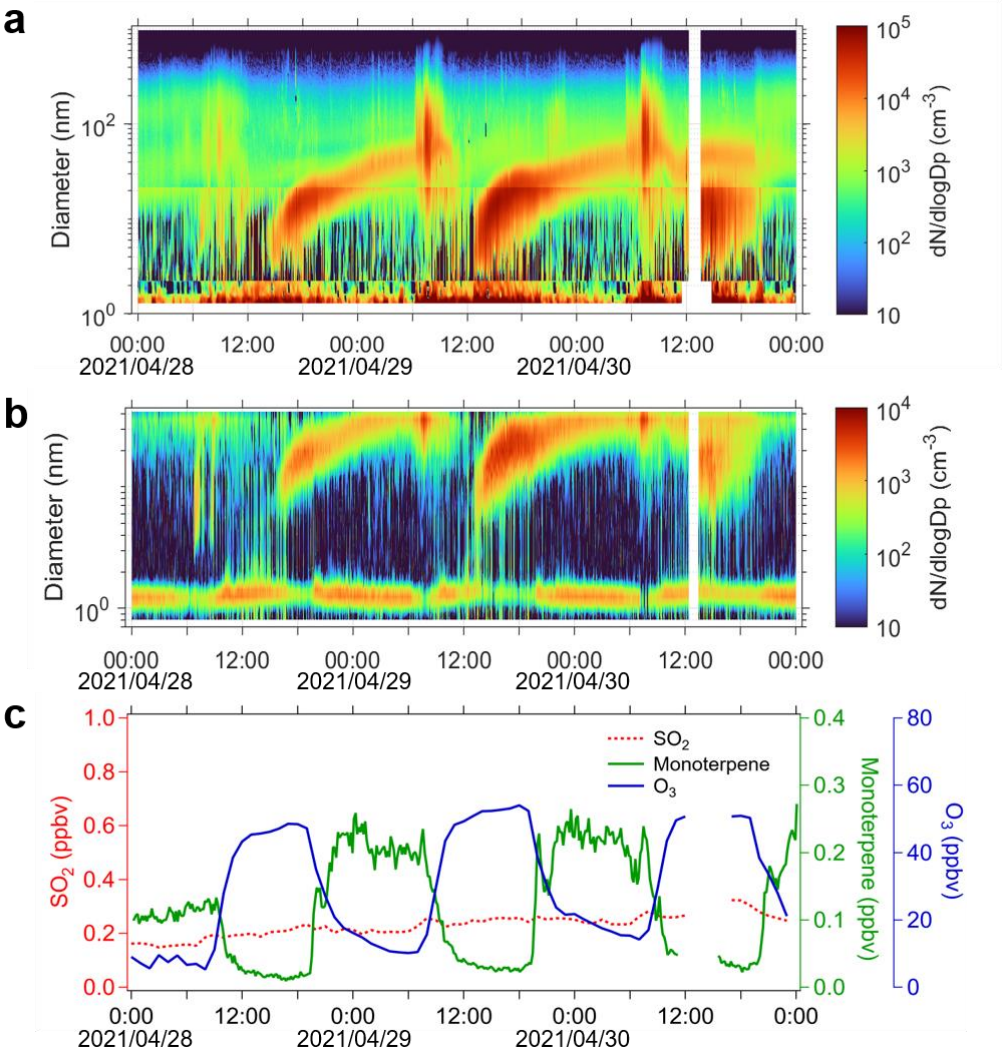

Fig. R2 Temporal evolution of (a) particle number size distribution from 1 nm to 1000 nm, (b) positive ion number size distribution from 0.8 nm to 40 nm. Note that the high peaks of number concentrations around 10–200 nm observed in the morning was caused by the wood burning in a residential cottage near the site. (c) SO_2, monoterpene and O_3 concentrations measured in Lulang site during 28–30 April, 2021. All time is in the UTC+8 time zone in this study.

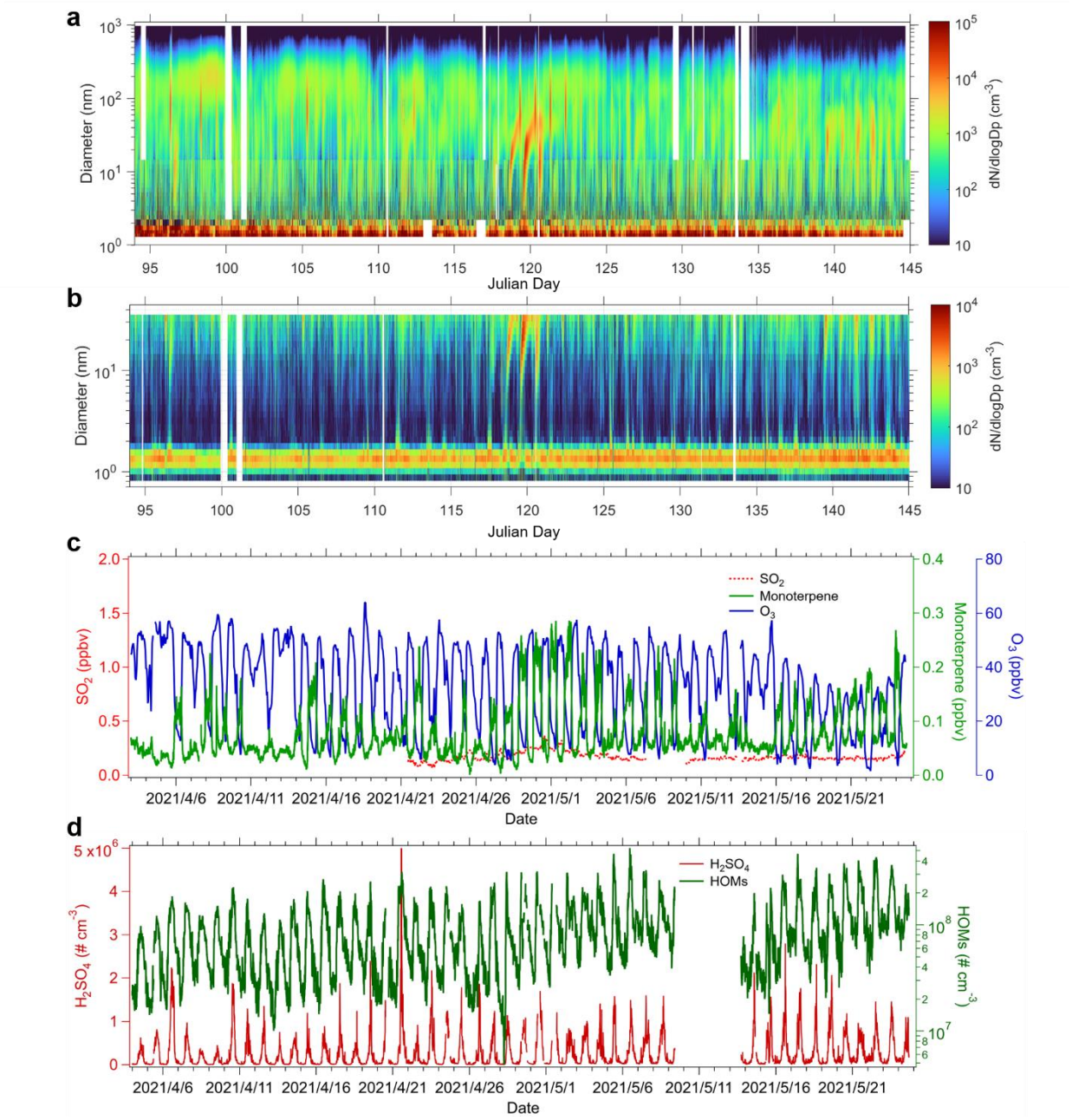

Fig. R3. Time series of (a) particle number size distribution from 1 nm to 1000 nm, (b) positive ion number size distribution from 0.8 nm to 40 nm, (c) SO_2, monoterpene and O_3 concentrations, (d) sulfuric acid and HOMs concentrations during the observation campaign in Lulang from 4 April to 24 May, 2021.

5. Figure 4c: As above, the sequence of greens is quite difficult to understand here. Also, is the choice of red + green for sulphuric acid + H_2SO_4 color blind friendly?

Response: Thanks for your comment. We have modified Fig. 4c considering color blind friendly (see Fig. R1).

6. Figure 5b,c: I'm finding these bar charts slightly hard to read. Why do the charts start at <10^1 cm^{-3}? It makes the actual difference quite hard to see. Why not a boxplot with a Y axis? Then we'd be able to see the min/max concentrations measured & predicted by the model, as well as the distribution, and median value.

Response: Thank you for the comment. We re-plotted Figure 5b,c using boxplots (see Fig. R4).

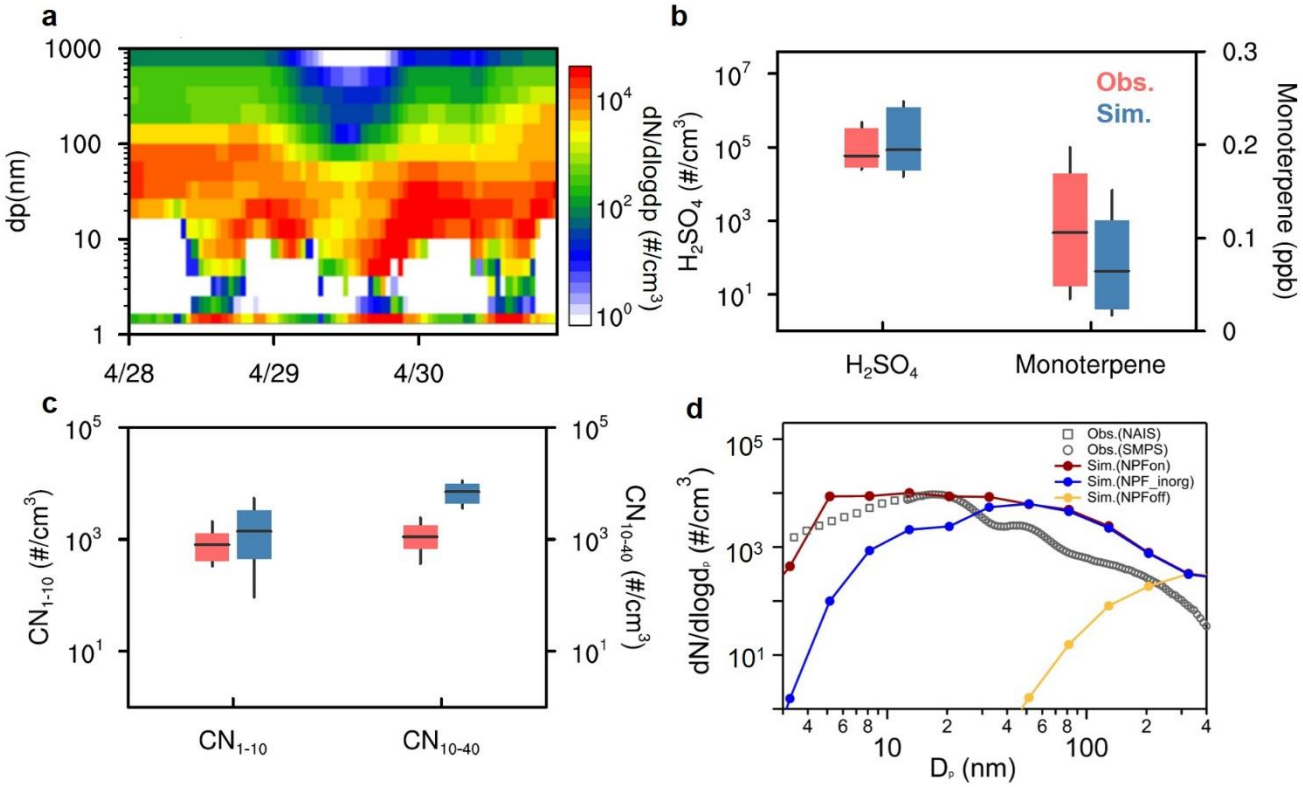

Fig. R4. (a) Simulated particle number size distribution in Lulang. (b) Observed and simulated H_2SO_4 and monoterpene concentration in Lulang. Bars are the median value during 28–30 April. The horizontal lines of box represent the 66th percentile, median and 33rd percentile and the whiskers represent the 75th and 25th percentiles. (c) Same as Fig. 5b but for number concentrations of 1–10 nm and 10–40 nm particles. (d) The observed and simulated particle number size distributions averaged from 12:00 to 18:00 during 28–30 April. The gray squares and gray circles show the measurements by NAIS and SMPS, respectively. Red, blue and orange lines represent the NPF-on, NPF_inorg and NPF-off experiments.

7. Figure 5d: It looks like there's a factor of 2-3 difference between the point where the NAIS and SMPS cross over. Do you have a reference instrument you can correct to? If not, it's common practice to correct the NanoSMPS/NAIS to the LongSMPS. In either case, it doesn't make any difference to the conclusions of the figure.

Response: Thank you for the comment. We corrected particle number size distribution observed by NAIS to the that observed by LongSMPS and re-plotted Fig. 5d (see Fig. R4).

8. Line 384: Do you mean "high values" rather than "certain values"?

Response: Thanks for your comment. Due to the strong atmospheric oxidizing capacity and low condensation sink (CS), H_2SO_4 concentrations can reach relatively high values, especially on the Tibetan Plateau (TP) compared to the surrounding areas. However, it's important to note that, in an absolute sense (or compared with the H_2SO_4 concentration in polluted environments), we do not consider the sulfuric acid concentration to be very high, as the average value is below 1 ppt.

Considering the referee's comments, we have modified the sentence in the revised manuscript (Lines 423–424).

9. Line 386 (and following paragraph): What about the SO_2? If that is also anthropogenic (which I'd presume it is as I doubt there's much DMS up there) then this strengthens your biogenic-anthropogenic argument.

Response: Thanks for your comment. Indeed, SO_2 is also of anthropogenic origin and aligns with NH_3 in its characteristics in the simulation. SO_2, primarily derived from coal combustion in power generation and industrial production, displays high concentrations in South Asia (as depicted in Fig. 7a). In addition to NH_3, the southerly winds during the daytime can also transport SO_2 to the TP, contributing to NPF over the TP. This additional information reinforces the biogenic-anthropogenic argument. The roles of DMS in H_2SO_4 formation were not considered as DMS was not observed and simulated in this study.

Considering the referee's comments, we have incorporated discussions about SO_2 in the revised manuscript (Lines 411–413 and Lines 432–434).

10. Figure 10: Is nucleation rate here J1.5, J3, or J10? Also, it might be easier to read if instead of "binary" and "ternary" you put H2SO4-H2O and H2SO4-NH3-H2O.

Response: Thank you for your comment. In this study, the nucleation rates presented in Figure 10 are based on parameterizations derived from the CLOUD experiments, specifically reporting nucleation rates at a mobility diameter of 1.7 nm. Therefore, strictly speaking, the nucleation rate in this study refers to $J_{1.7}$. Considering the referee's points, we clarified in Figure 10 that the nucleation rate corresponds to $J_{1.7}$ in the revised manuscript (see Fig. R5). We also modified the "binary" and "ternary" to "H_2SO_4-H_2O" and "H_2SO_4-NH_3-H_2O" in the revised manuscript.

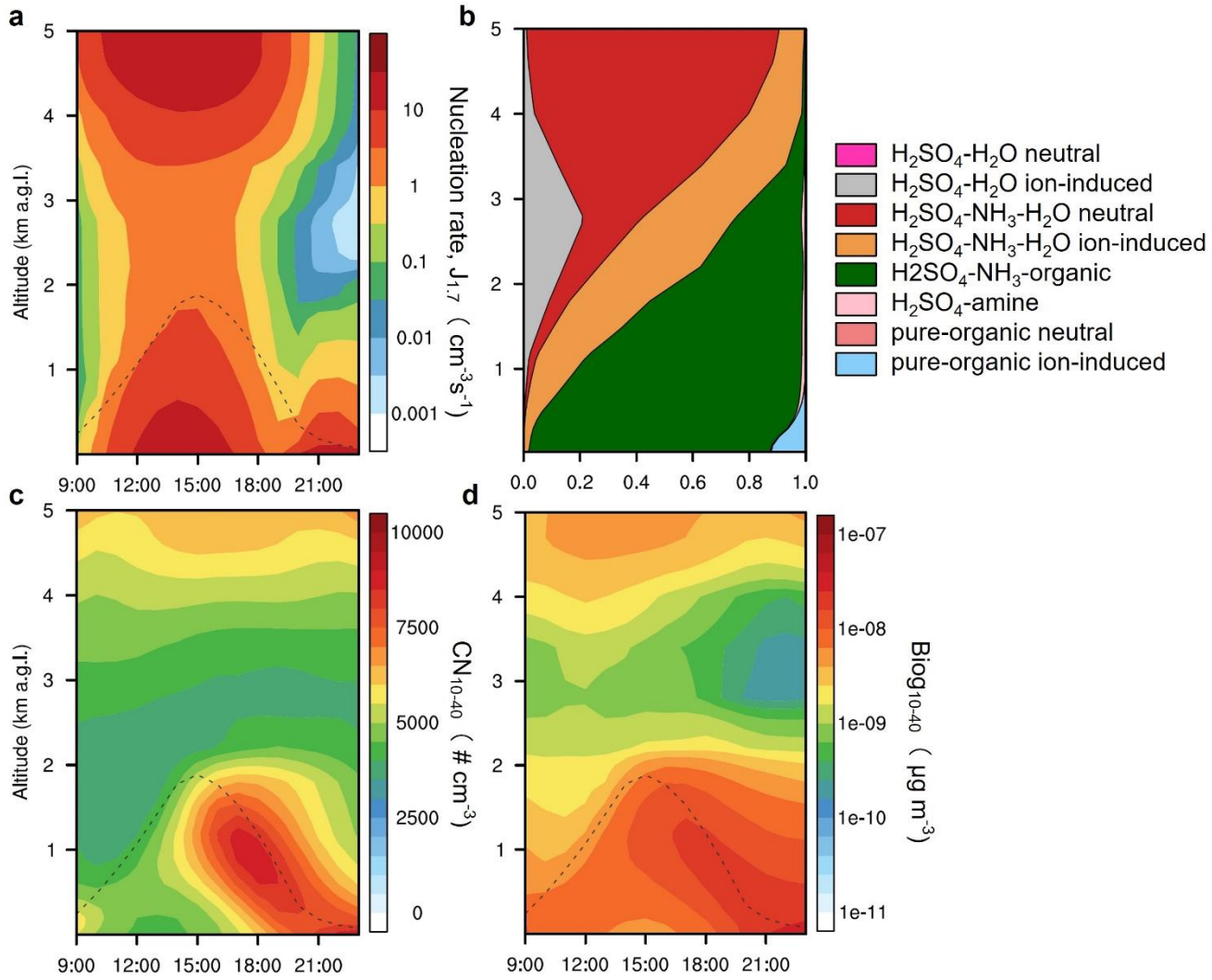

Fig, R5. (a) Averaged diurnal evolution of vertical cross section of simulated nucleation rate ($J_{1.7}$) over the research domain during 28–30 April. Note: The black dashed line shows the planetary boundary layer height (PBLH). (b) The relative contribution of different NPF pathways averaged over the research domain during 28–30 April. (c) Same as Fig. 10a but for 10–40 nm particle number concentrations. (d) Same as Fig. 10a but for 10–40 nm biogenic organic mass concentrations.

11. Line 461: What fraction of total CN10-40 mass does this Biogenic organic mass comprise?

Response: Thanks for your comment. The biogenic organic mass comprises 17% of the total CN_{10-40} mass in our simulation. The concentration of pre-existing particles is overestimated due to the uncertainties in the emission inventories. Therefore, the model could underestimate the biogenic organic mass in the size range 10-40 nm as the HOMs from biogenic sources could condense on large particles.

12. Line 462: Maybe worth considering that autoxidation rates also decrease with temperature (5)

Response: Thanks for your comment. Indeed, the temperature-dependent factors influencing the condensation process of organic vapors are complex. While autoxidation rates tend to decrease with temperature, the volatility of organics also decreases at lower temperatures, introducing a competing effect (Stolzenburg et al., 2018).

In our study, we found that changes in volatility play a leading role in the PBL. Consequently, the lower temperature at higher altitudes (Fig. S1c) creates more favorable conditions for the condensation process of organic vapors, leading to the counter-gradient of biogenic organic mass (Fig. 10d) and contributing to the

subsequent growth of nanoparticles.

We have added the discussions on the temperature-dependence of autoxidation rates in the revised manuscript (Lines 506–508).

1. *L. Pichelstorfer et al., Towards a mechanistic description of autoxidation chemistry: from precursors to atmospheric implications. EGUsphere **2023**, 1-30 (2023).*
2. *C. Rose et al., Observations of biogenic ion-induced cluster formation in the atmosphere.*
   *Science Advances **4**, eaar5218.*
3. *K. Lehtipalo et al., Multicomponent new particle formation from sulfuric acid, ammonia, and biogenic vapors. Science Advances **4**, eaau5363.*
4. *C. Mohr et al., Molecular identification of organic vapors driving atmospheric nanoparticle growth. Nature Communications **10** (2019).*
5. *D. Stolzenburg et al., Rapid growth of organic aerosol nanoparticles over a wide tropospheric temperature range. Proceedings of the National Academy of Sciences **115**, 9122-9127 (2018).*

References

Beddows, D. C. S.; Dall'osto, M. , and Harrison, R. M.: An Enhanced Procedure for the Merging of Atmospheric Particle Size Distribution Data Measured Using Electrical Mobility and Time-of-Flight Analysers, Aerosol Sci. Technol., 44, 930-938, 10.1080/02786826.2010.502159, 2010.

Dunne, E. M.; Gordon, H.; Kurten, A.; Almeida, J.; Duplissy, J.; Williamson, C.; Ortega, I. K.; Pringle, K. J.; Adamov, A.; Baltensperger, U., et al.: Global atmospheric particle formation from CERN CLOUD measurements, Science, 354, 1119-1124, 10.1126/science.aaf2649, 2016.

Ehn, M.; Thornton, J. A.; Kleist, E.; Sipila, M.; Junninen, H.; Pullinen, I.; Springer, M.; Rubach, F.; Tillmann, R.; Lee, B., et al.: A large source of low-volatility secondary organic aerosol, Nature, 506, 476-479, 10.1038/nature13032, 2014.

Heinritzi, M.; Simon, M.; Steiner, G.; Wagner, A. C.; Kürten, A.; Hansel, A. , and Curtius, J.: Characterization of the mass-dependent transmission efficiency of a CIMS, Atmospheric Measurement Techniques, 9, 1449-1460, 10.5194/amt-9-1449-2016, 2016.

Jokinen, T.; Sipila, M.; Junninen, H.; Ehn, M.; Lonn, G.; Hakala, J.; Petaja, T.; Mauldin, R. L.; Kulmala, M. , and Worsnop, D. R.: Atmospheric sulphuric acid and neutral cluster measurements using CI-APi-TOF, Atmos. Chem. Phys., 12, 4117-4125, 10.5194/acp-12-4117-2012, 2012.

Kulmala, M.; Petaja, T.; Nieminen, T.; Sipila, M.; Manninen, H. E.; Lehtipalo, K.; Dal Maso, M.; Aalto, P. P.; Junninen, H.; Paasonen, P., et al.: Measurement of the nucleation of atmospheric aerosol particles, Nat Protoc, 7, 1651-1667, 10.1038/nprot.2012.091, 2012.

Kulmala, M.; Kontkanen, J.; Junninen, H.; Lehtipalo, K.; Manninen, H. E.; Nieminen, T.; Petaja, T.; Sipila, M.; Schobesberger, S.; Rantala, P., et al.: Direct observations of atmospheric aerosol nucleation, Science, 339, 943-946, 10.1126/science.1227385, 2013.

Kürten, A.; Rondo, L.; Ehrhart, S. , and Curtius, J.: Calibration of a Chemical Ionization Mass Spectrometer for the Measurement of Gaseous Sulfuric Acid, Journal of Physical Chemistry A, 116, 6375-6386, 10.1021/jp212123n, 2012.

Kürten, A.; Bianchi, F.; Almeida, J.; Kupiainen-Määttä, O.; Dunne, E. M.; Duplissy, J.; Williamson, C.; Barmet, P.; Breitenlechner, M.; Dommen, J., et al.: Experimental particle formation rates spanning tropospheric sulfuric acid and ammonia abundances, ion production rates, and temperatures, Journal of Geophysical Research: Atmospheres, 121, 10.1002/2015jd023908, 2016.

Lehtipalo, K.; Yan, C.; Dada, L.; Bianchi, F.; Xiao, M.; Wagner, R.; Stolzenburg, D.; Ahonen, L. R.; Amorim, A.; Baccarini, A., et al.: Multicomponent new particle formation from sulfuric acid, ammonia, and biogenic vapors, Science Advances, 4, 9, 10.1126/sciadv.aau5363, 2018.

Riccobono, F.; Schobesberger, S.; Scott, C. E.; Dommen, J.; Ortega, I. K.; Rondo, L.; Almeida, J.; Amorim, A.; Bianchi, F.; Breitenlechner, M., et al.: Oxidation products of biogenic emissions contribute to nucleation of atmospheric particles, Science, 344, 717-721, 10.1126/science.1243527,

2014.
Roldin, P.; Ehn, M.; Kurten, T.; Olenius, T.; Rissanen, M. P.; Sarnela, N.; Elm, J.; Rantala, P.; Hao, L. Q.; Hyttinen, N., et al.: The role of highly oxygenated organic molecules in the Boreal aerosol-cloud-climate system, Nat. Commun., 10, 15, 10.1038/s41467-019-12338-8, 2019.
Schervish, M. , and Donahue, N. M.: Peroxy radical chemistry and the volatility basis set, Atmos. Chem. Phys., 20, 1183-1199, 10.5194/acp-20-1183-2020, 2020.
Sihto, S. L.; Kulmala, M.; Kerminen, V. M.; Dal Maso, M.; Petäjä, T.; Riipinen, I.; Korhonen, H.; Arnold, F.; Janson, R.; Boy, M., et al.: Atmospheric sulphuric acid and aerosol formation: implications from atmospheric measurements for nucleation and early growth mechanisms, Atmos. Chem. Phys., 6, 4079-4091, 10.5194/acp-6-4079-2006, 2006.
Stolzenburg, D.; Fischer, L.; Vogel, A. L.; Heinritzi, M.; Schervish, M.; Simon, M.; Wagner, A. C.; Dada, L.; Ahonen, L. R.; Amorim, A., et al.: Rapid growth of organic aerosol nanoparticles over a wide tropospheric temperature range, Proc Natl Acad Sci U S A, 115, 9122-9127, 10.1073/pnas.1807604115, 2018.